Simulated Structure Factors

Benjamin J. Coscia

July 13, 2018

1 Calculation of the structure factor

The structure factor, S($\mathbf{q}$), relates the observed intensity per atom to that observed by a single scattering unit. Incident plane waves falling on a material have a wave vector, K_i, whose length is $\frac{2\pi}{\lambda}$, where λ is the wavelength. The diffracted wave vector, K_f, has the same length as K_i if the diffraction process is elastic. We will assume elasticity going forward. The scattering vector, $\mathbf{q}$, is defined as $K_f - K_i$. Since K_f and K_i are the same length, the scattering vector must lie on the surface of a sphere of radius $\frac{2\pi}{\lambda}$. This sphere is called the Ewald Sphere and diffraction will only occur for reciprocal lattice points that lie on its surface.

The amplitude and phase of the scattered waves is the vector sum of all scattered waves from all atoms:

$$\Psi_s(\mathbf{q}) = \sum_{j=1}^{N} f_j e^{-i\mathbf{q}\cdot\mathbf{R_j}} \tag{1}$$

where f_j is the atomic form factor of atom j and $\mathbf{R_j}$ is the position of the atom in real space. Note that Equation 1 is the definition of the discrete fourier transform.

The scattered intensity is obtained by multiplying Equation 1by its complex conjugate:

$$I(\mathbf{q}) = \Psi_s(\mathbf{q}) \cdot \overline{\Psi_s}(\mathbf{q}) = \sum_{j=1}^{N} f_j e^{-i\mathbf{q}\cdot\mathbf{R_j}} \times \sum_{k=1}^{N} f_k e^{-i\mathbf{q}\cdot\mathbf{R_k}} = \sum_{j=1}^{N}\sum_{j=k}^{N} f_j f_k e^{-i\mathbf{q}\cdot(\mathbf{R_j}-\mathbf{R_k})} \tag{2}$$

Computationally, one should calculate the fourier transform of the atomic coordinates with a fast fourier transform, calculate its complex conjugate and multiply them together. The structure factor is typically normalized as $1/\sum_{j=1}^{N} {f_j}^2$ so that it is independent of system size, and the general equation for the structure factor becomes:

$$S(\mathbf{q}) = \frac{1}{\sum_{j=1}^{N} {f_j}^2} \sum_{j=1}^{N}\sum_{j=k}^{N} f_j f_k e^{-i\mathbf{q}\cdot(\mathbf{R_j}-\mathbf{R_k})} \tag{3}$$

If all atoms are identical, Equation 2 simplifies to:

$$S(\mathbf{q}) = \frac{1}{N} \sum_{j=1}^{N}\sum_{j=k}^{N} e^{-i\mathbf{q}\cdot(\mathbf{R_j}-\mathbf{R_k})} \tag{4}$$

The atomic form factor, f_j is more complicated than how it is represented in Equation 1 The atomic form factor is the scattering contribution from a single isolated atom. They are calculated as the fourier transform of the electron density, $\rho(\mathbf{r})$, which is typically calculated using quantum techniques. Since $\rho(\mathbf{r})$ is a spatially dependent function, f_j is actually a function of $\mathbf{q}$, $f(\mathbf{q})$. Values of $f(\mathbf{q})$ for each element are tabulated in the International Tables for Crystallography. For $\mathbf{q} = \mathbf{0}$, the atomic form factor is equal to the number of electrons possessed by the atom.

The resolution in each dimension of reciprocal space is determined by the size of the unit cell studied. In order to calculate the structure factor, the system's 3D coordinates must be discretized into regularly sampled points using a histogramming method. Applying equation 2 to the histogram will yield a grid with

Fourier bin sizes of $\frac{2\pi}{L_i}$ (i = (x,y,z)). The fourier transform of an array of values returns a same length array of frequencies. Increasing the number of bins in the histogram will not change the size of the Fourier space bins, rather it will increase the maximum accessible value of q.

2 Structure factor of hexagonally packed columns

Here, we explore, in depth, a simplified model of an inverted hexagonal phase lyotropic liquid crystal (H_{II} LLC). The simplified model is meant to enhance our understanding of the structure factor of a fully atomistic model of the same material. We are primarily interested in the diffraction patterns produced by the head groups so we model each monomer as a point placed at the center of mass of its head group. The hexagonal phase is made of straight pore columns. Each pore column is composed of columns of stacked monomers which surround the pore's hydrophilic core. Based on simulation, there are likely 5 monomer columns making up each pore, and the pore radius is ca. 1 nm. Experimental WAXS suggests that monomers stack 3.7 Åapart, and SAXS measurements have shown that pores are spaced ca. 4.1 nm apart. Here, unless otherwise noted we took the pore spacing to be 4.25 nm for no good reason. For consistency with simulation, we will look at 4 pores in a monoclinic unit cell with 5 monomer columns per pore, unless specified otherwise.

We are interested in the intensity and dimensions of the R-π reflection, which is a consequence of monomers stacked on top of each other in the z-direction.

2.1 Crystalline liquid crystals

NEW There are two ways to set up the pores for this system. The first is to make all pores exactly the same; just copies that are translated to different pore locations (Figure 1a). It is not clear whether a perfect crystal of this material would be arranged in this way. The second way is to randomly rotate each pore (Figure 1b). In this work we use the latter.

(a) (b)

Figure 1: A top-down (xy) view of the pore columns. (a) The right pore is an exact duplicate of the left including rotation about the z-axis. (b) The right pore is a duplicate of the left pore but rotated a random amount about the z-axis.

For a perfect, infinite crystal, the intensity of R-π is infinitely sharp. We created a model with perfectly aligned columns. Each columns originates at z=0 and all other points in the column are equally spaced 3.7 Å apart in the z-direction (Figure 2). This essentially creates layers of atoms. The intensity of R-π for systems of various size are shown in Table 1. The intensity of R-π is equal to the number of atoms in the unit cell. The intensity will approach infinity as the system size becomes infinitely large.

We measured the peak width of R-π in the q_r direction using the appropriate slice of the structure factor. Ideally, one should use the angle averaged structure factor for this calculation, but since the angle averaging procedure interpolates between bins, the averaged intensities are lower than expected which slightly changes

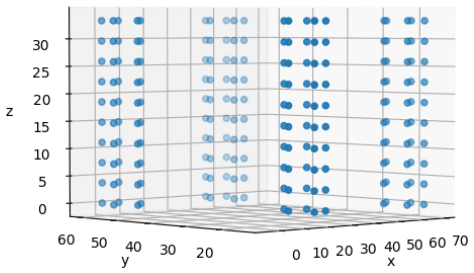

Figure 2

L_z (Å)	Points per column	Number of Pores	Number of Atoms	R-π Intensity
14.8	4	4	80	80
18.5	5	4	100	100
37	10	4	200	200
14.8	4	9	180	180
18.5	5	9	225	225
37	10	9	450	450
14.8	4	16	320	320
18.5	5	16	400	400
37	10	16	800	800

Table 1: The intensity of R-π in a perfect crystal is equal to the number of scatterers in the unit cell. Here, L_z is the length of the unit cell in the z direction which corresponds to number of points per column $\times$ 3.7.

the shape of the peak and gives misleading results. This reflection is radially symmetric about the z-axis, so we fit peak widths to cross-sections at $(0, y, 1.7)^{-1}$ Å(See Figure 3).

The distance, d, between peaks in the q_y cross-sections of the structure factor is equal to $2\pi/d$ (Figure 3). We looked at systems with pores spaced 42.5 nm and 212.5 nm apart respectively. The fundamental frequency appears at $q_y = 0$ with magnitude equal to the number of atoms in the unit cell (Note that each system has a different number of atoms). Subharmonics follow the fundamental frequency at equally spaced intervals of width $2\pi/d$.

We quantified the peak width by fitting gaussian curves to the R-π peak cross-sections and measuring ther full width at half maximum. Gaussian profiles appear to give the closest fit to the data (see Figure 4). We calculated all of FWHMs in Table 1 using gaussian fits.

IMPORTANT: Note that these 'peak widths' are not the same peak widths that are seen experimentally. If these showed up experimentally, they would appear as dots parallel to the q_r axis, crossing through R-π and in line with R-pores. There is some evidence of this occuring in some of the simulations (ordered parallel displaced for example).

The distance between pores does not affect the FWHM of the R-π 'peak' in the q_y direction. We held the size of the unit cell constant at 42.5 x 42.5 x 3.7 nm and varied the number of pores (and consequently, the distance between pores). We generated error bars for the fits based on the covariance of the optimized fit parameters. There is no statistical difference between the calculated values of each FWHM (Table 4). The uncertainty is lower for systems with less pores since there are more subharmonics available for curve fitting.

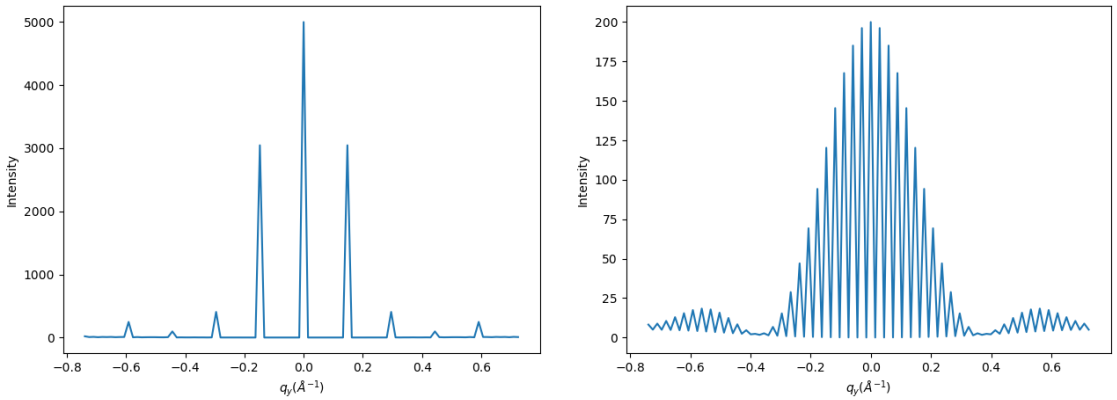

Figure 3: The distance between peaks of the structure factor cross-section at (0, y, 1.7) is equal to the distance between pores in q-space. The center peak of each distribution shows the fundamental frequency. The peaks that follow at higher $|\mathbf{q}|$ values are subharmonics. Both systems shown are in unit cells with dimensions of 42.5 x 42.5 x 3.7 nm. (a) We held the pore-to-pore spacing constant at 42.5 Å. The unit cell consists of 100 total pores. The first peak off-center peak is located at $q_y = .148\mathring{A}^{-1}$ which corresponds to $2\pi/.148 = 42.5\mathring{A}$ in real space. (b) We placed four pores in a unit cell spaced 212.5 Å apart. The first peak appears where expected at $q_y = 0.0296\mathring{A}^{-1}$ $(2\pi/212.5\mathring{A})$ and all other peaks are separated by that same distance.

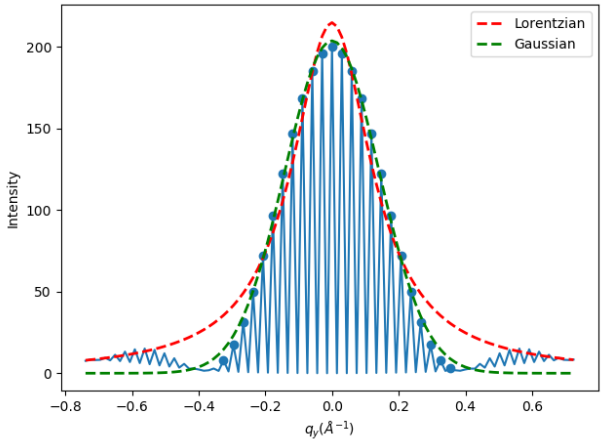

Figure 4: The gaussian functional form more closely matches the data than the Lorentzian functional form. Shown is data for a perfect crystal system with 4 pores and 4 points per column.

L_z (Å)	Number of Pores	Distance between Pores	R-π intensity	FWHM ($\mathring{A}^{-1}$)
37	4	212.5	200	0.372 ± 0.004
37	25	85.0	1250	0.371 ± 0.008
37	100	42.50	5000	0.375 ± 0.013

Table 2: We held the size of the unit cell constant at 42.5 x 42.5 x 3.7 nm and varied the number of pores and distance between pores. The value of FWHM is indistinguishable between the systems.

The finite FWHM of perfectly crystalline systems is due to non-uniform ordering of the columns within the pores. Although all scatterers are aligned and equally spaced in the z-direction, the individual columns of scatterers are offset from the pore center. Therefore, there is a range of similar but different distances

between scatter scatterers. There are many opportunities for constructive and destructive interference with wavelengths slightly different than those which contribute to the fundamental frequency. If we place only one column at each pore center, the FWHM becomes infinite (See Figure 5)

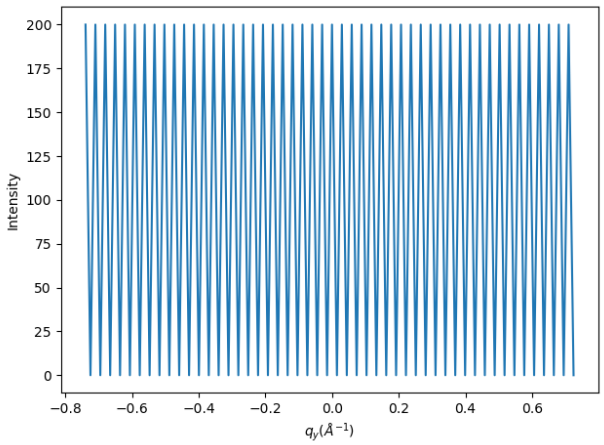

Figure 5: We placed one column of scatterers at each of 4 pore centers, spaced apart by 212.5 nm. Since the y-component of the distance between all scatterers is the same in all cases, subharmonics appear just as strongly as the fundamental frequency. Since the intensity doesn't decay, the FWHM is infinite.

The real system is far from a perfect crystal. Here we explore the influence of 4 sources of disorder on the intensity of R-π:

1. Random z-displacement of columns with respect to all other columns
2. Random rotation of layers about the z-axis
3. Thermal noise
4. Finite correlation between scatterers in the z-direction

2.2 Imperfectly aligned columns

We randomly aligned columns along the z-axis by adding a random displacement to each column of points. This simulates a system in which columns are uncorrelated. We wrapped coordinates where necessary so that all atoms stayed within the unit cell. We held the spacing between each point within each column at 3.7 Å. We created trajectories of 1000 independent configurations in order to calculate the average intensity of R-π. 1000 independent configurations gives a reasonably converged average, enough to observe trends.

NEW We varied the degree to which we shifted each column with respect to other columns. The most we allowed the columns to shift was one full layer. To choose the position of the column, we chose a random displacement between 0 and d, where d is the maximum allowed displacement. We varied d between 0 and 3.7 Å.

When d = 3.7 Å, the intensity of R-π is equal to the number of scatterers per column (See Table 4). It is independent of the number of pores (and hence number of columns) in the system. The error in the calculated intensities are comparable to the magnitude of the intensity because the intensity of each configuration in the trajectory fluctuates so much.

NEW As we allow the columns to displace less (lower values of d), the intensity of R-π increases (See Figure 6). Once there is no displacement, the intensity of R-π matches that of a perfect crystal. The intensity of R-π in our system is likely boosted by correlation between columns.

The q_y width of R-π is infinite when columns are randomly displaced in the z-direction. We attempted to measure the FWHM of the system with randomly displaced columns containing 4 pores and $L_z = 37$. The cross-section (Figure 7a) shows non-decaying noise centered near 10, the same R-π intensity in Table 4.

L_z (Å)	Points per column	Number of Pores	R-π Intensity
14.8	4	4	3.98
18.5	5	4	5.05
37	10	4	10.08
14.8	4	9	4.06
18.5	5	9	4.78
37	10	9	10.19
14.8	4	16	4.01
18.5	5	16	4.95
37	10	16	9.61

Table 3: The intensity of R-π is equal to the number of scatters in each column when columns are uncorrelated.

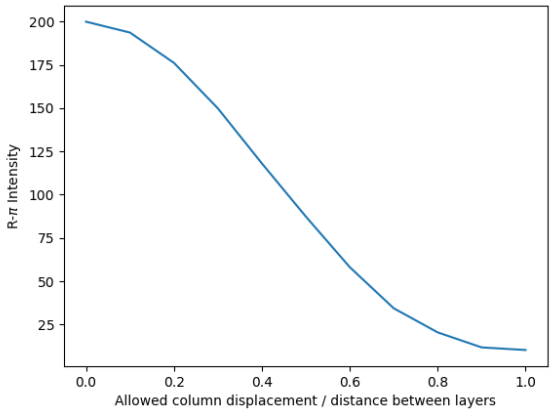

Figure 6: As we increase the amount that columns are allowed to displaced relative to each other, the intensity of R-π decreases.

The angle averaged pattern (Figure 7b) further illustrates the diffraction lines which characterize this type of system.

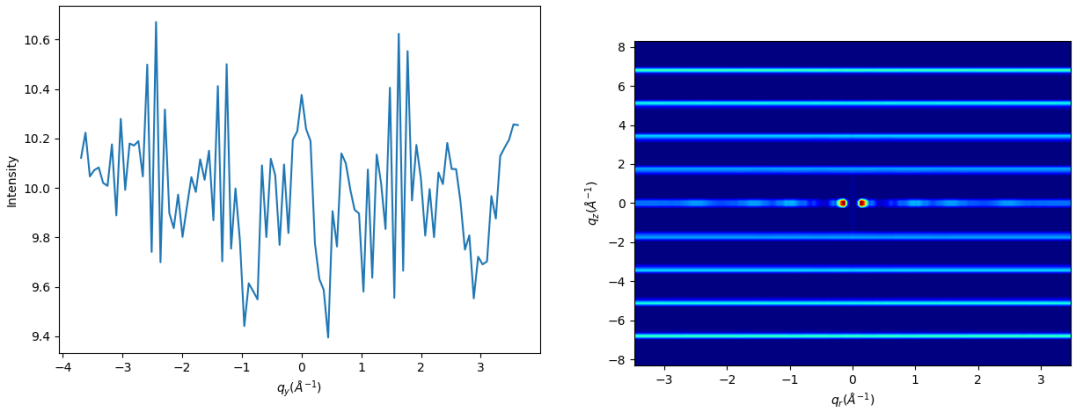

(a) (b)

Figure 7

2.3 Randomly rotated layers

We observed the influence of correlation between layers by randomly rotating layers of scatterers about the z-axis. We held constant the angle, with respect to the pore center, between scatterers for any given layer. For example, since there are 5 columns per pore, each layer is made of 5 monomers. The angle made between the two vectors extending from the pore center to two adajacent scatterers in a single layer is 72 ° with respect to the xy plane.

L_z (Å)	Points per column	Number of Pores	Number of Atoms	R-π Intensity	FWHM $\mathring{A}^{-1}$
14.8	4	4	80	80	0.37
18.5	5	4	100	100	0.37
37	10	4	200	200	0.37
14.8	4	9	180	180	0.37
18.5	5	9	225	225	0.37
37	10	9	450	450	0.37
14.8	4	16	320	320	0.37
18.5	5	16	400	400	0.37
37	10	16	800	800	0.37

Table 4: The intensity of R-π is equal to the number of scatters in each column when columns are uncorrelated. Note that reproducing these results requires a very fine histogram, and thus a much more expensive calculation. The default binning scheme (100 bins in each dimension) gives slightly misleading answers.

In all cases, the maximum intensity of R-π is equal to the number of scatterers in the system and the FWHM of the q_y cross-section of the structure factor at R-π is 0.37 $\mathring{A}^{-1}$, just as the perfect crystal.

NEW There is no major difference in the intensity of R-π between a perfect crystal and a system with randomly rotated layers. In the z direction, R-π remains constant since the z components of the points are spaced exactly 3.7 Åapart. The maximum intensity of R-π is at $(q_x, q_y, q_z) = (0, 0, 1.7)$ so there is no contribution from the x or y components. Figure 8a shows a comparison of the cross-section of R-π along $q_y = 0$. On the surface it appears that there is a difference between them at high values of q_y. However, this is dependent on the initial configuration of the perfect crystal system. The system with randomly rotated layers will always look as it does if a sufficient number of configurations are included in the calculation of the structure factor. The perfect system is in agreement with the randomly rotated layer system at low values of q_y, corresponding to scatteres spaced far apart, however it begins to deviate at large q_y, where it describes the spatial relationship between scatterers in a single pore. In the perfect system, pores are randomly rotated with respect to each other (See Figure 1a), so the spatial relationship changes each time a system is set up. It will not average out since each frame is exactly the same, but if enough pores are added, the 2 cross-sections will match (See Figure 8b). If we create a perfect crystal system where pores are duplicated and translated, but not rotated (See Figure 1a), the subharmonics at large q_y are quite pronounced (Figure 8c) due to the increase in ordering in the q_y direction. The peaks are likely geometrically related to the spacing between points within pores, but it is not important to get to the bottom of that here.

2.4 The influence of thermal disorder

We added gaussian noise in each dimension to observe its influence on the intensity of R-π and the FWHM. For the z-direction, the standard deviation of the gaussian distribution is equal to a fraction of the average distance between scatterers in columns (d). In the xy-directions, the standard deviation is equal to a fraction of the pore radius (r).

2.4.1 NEW Perfect Crystal

When we add z-direction gaussian noise to the lattice sites in the perfect crystal, the intensity of R-π drops precipitously as noise is increased (Figure 9a). However, the FWHM in the q_y direction is not affected by this noise.

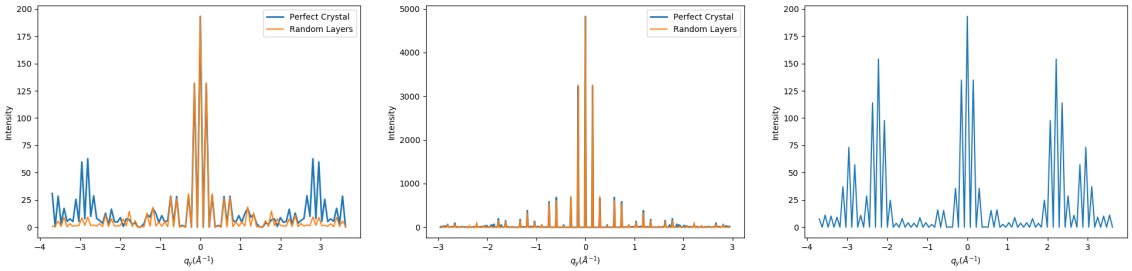

(a) (b) (c)

Figure 8: **NEW** Shown are cross-sections of the 3D structure factor along q_y at the q_z value of R-π. We compare the cross-section for a perfect crystal system and a system where layers are randomly rotated with respect to vertically adjacent layers. (a) When systems are made with 4 pores, the cross-sections agree at low q_y values, however they diverge at higher values of q_y. (b) When we build the systems with 100 pores, the cross-sections are in close agreement. (c) If we do not rotate the pores in the perfect crystal system, there are large spikes at high values of q_y due to order within pores.

When we add gaussian noise in the x and y directions, the intensity of R-π does not change, however the FWHM sharpens with increasing noise (Figure 9b).

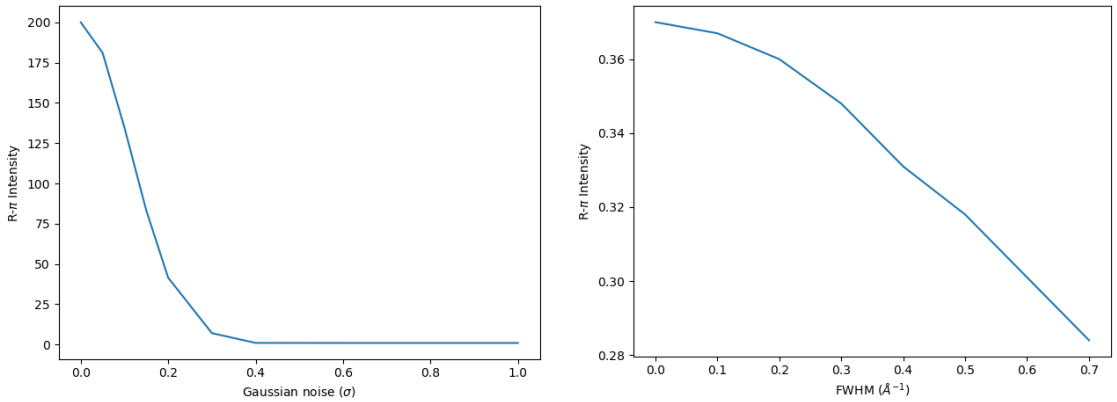

(a) (b)

Figure 9: (a) The intensity of R-π decreases as the amount of z-direction noise increases. (b) The FWHM decreases as noise in the x and y directions increases.

2.4.2 Randomly displaced columns

When we add noise in the z direction, the intensity of R-π decays (Figure 10a).

When we add noise in the x and y directions, R-π has a finite peak width in its q_y dimension (Figure 10b), and the intensity stays constant. We fit a Gaussian function to the the q_y cross-section in order to determine its FWHM. The FWHM decay is inversely proportional to the amount of noise added (Figure 10c).

This mode of broadening of R-π is more consistent with the experimental pattern, where the q_y cross-section of R-π is a continuous, broad peak.

2.4.3 Randomly rotated layers

When we add noise in the z direction, the intensity of R-π decays to 1 rapidly (Figure 11a), much like the decay shown in Figure 10a. The FWHM slowly increases until it jumps to infinity when the intensity of R-π is comparable to the background intensity.

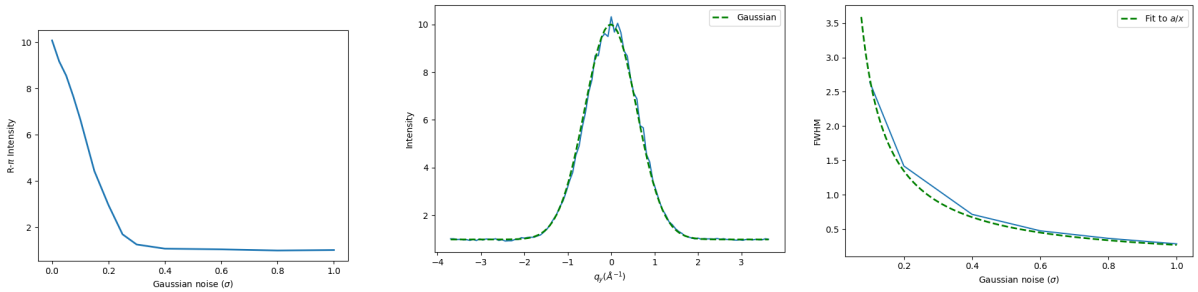

(a) (b) (c)

Figure 10: (a) The intensity of R-π decays to 1 rapidly as gaussian noise is added to the system. (b) When we add noise in the x and y directions, R-π broaden in the y-direction with a continuous intensity distribution that can be fit to a gaussian. (c) This FWHM decreases as the inverse of the amount of noise added.

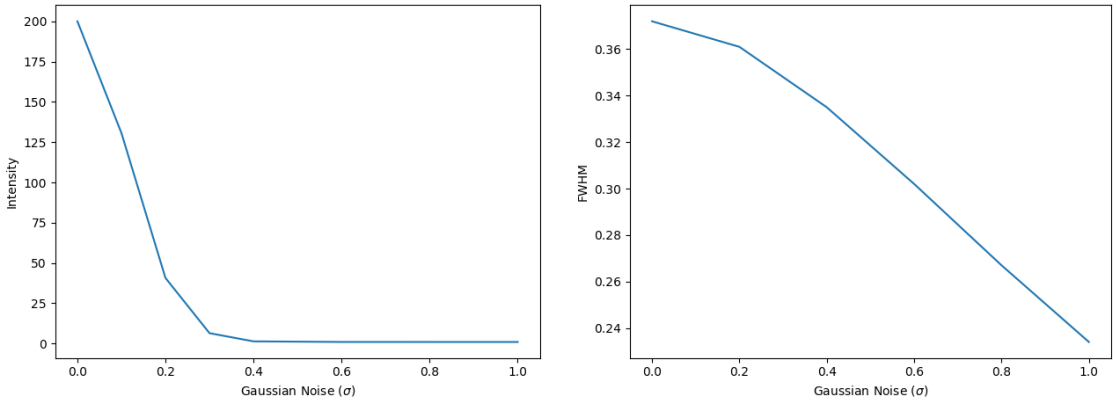

(a) (b)

Figure 11: (a) As we add noise in the z-direction, the intensity of R-π decreases rapidly to 1. The FWHM decays slowly and then jumps goes to infinity (not pictured) when the intensity of R-π becomes equal to the background intensity. However one could argue there is no peak at that point. (b) When we add noise in the x and y directions, the intensity of R-π does not change, but the FWHM decays slowly.

When we add noise in the x and y directions, the intensity of R-π does not change. The FWHM slowly decays as shown in Figure 11b. Importantly, the peak is defined by spikes like those shown in Figure 3.

2.4.4 Finite z-correlations

The z-cross-section of the R-π peaks are delta functions in all of the above systems (See Figure 13). None of the routes explored so far show how R-π might broaden in the q_z direction. The delta-function behavior does not change when the system is made taller so as to increase the resolution in z. We built a system 10x taller (37 nm), added random column displacement and some noise in the z-direction. R-π is still a sharp delta function (Figure 14).

(Please let me know if there is a more correct way of doing this) We added a correlation length to scatterers in z-direction. To do so, we define a covariance matrix to describe the correlation between all pairs of scatterers. The variance is defined so that the covariance in position of a scatterer with itself is the same for all scatterers. The covariance in position between scatterers decays exponentially from v according to the equation $ve^{-z/L}$ where L is the correlation length. Note that in its current implementation, it does not take periodicity into account, so a correlation length shorter than the box is necessary. A visualization of a typical covariance matrix for a column containing 20 scatterers is shown in Figure 15. Next, we drew

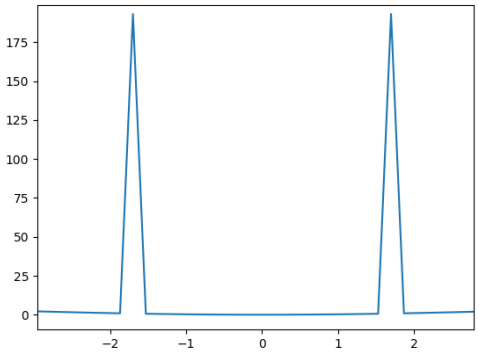

(a) Perfect Crystal

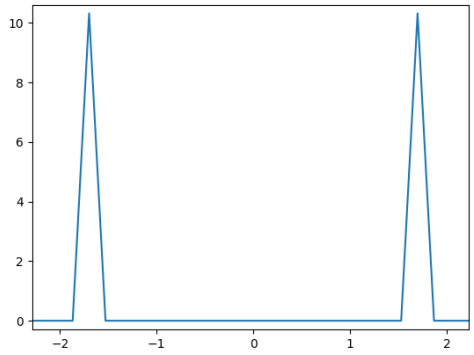

(b) Randomly displaced columns

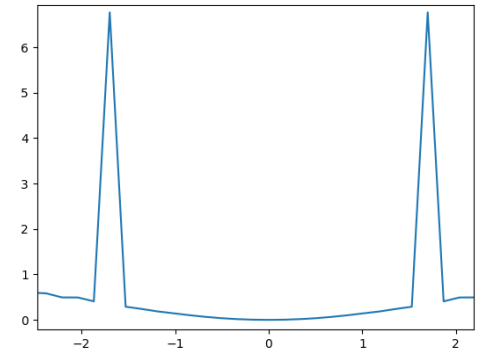

(c) Randomly displaced columns w/ z-noise

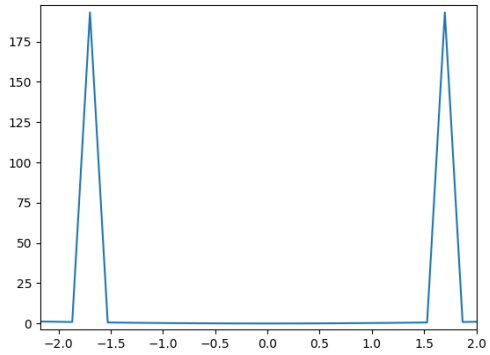

(d) Randomly rotated layers w/ xy-noise

Figure 12: Several examples of the delta-like behavior of R-π. Randomly displacing columns, randomly rotating layers, and adding thermal disorder do not broaden the z-cross-section of R-π.

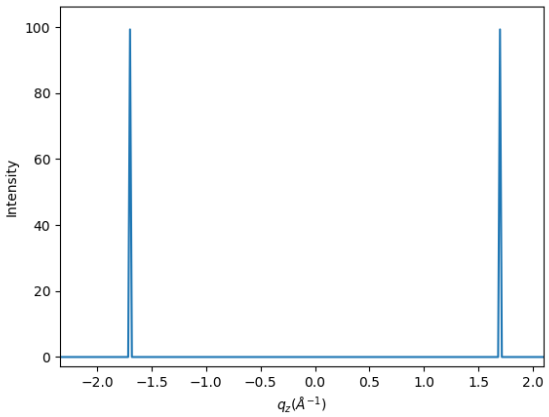

Figure 13: R-π still appears to be a delta function even with higher resolution and noise in the z-positions of the scatterers

random samples from a multivariate normal distribution defined using the covariance matrix, and applied these shifts to the columns of scatterers.

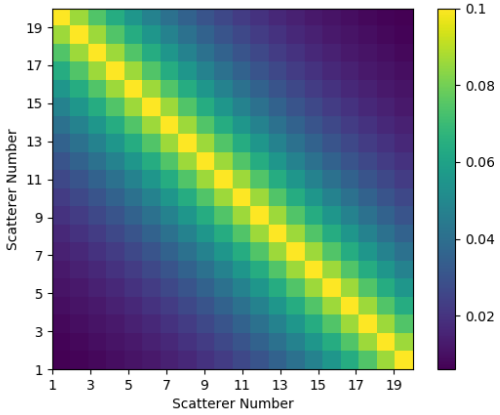

Figure 14

Adding a finite correlation length between scatterers causes R-π to broaden in the q_z direction. We simulated a system with dimensions of 8.5 x 8.5 x 37 nm, so that there would be 100 scatterers in the z-direction and a fourier bin size of $1/370 = 0.0027\AA^{-1}$. There is a clear broadening of R-π when scatterers are correlated (Figure 16a). The maximum intensity of R-π decreases as the variance in scatterer position increases (Figure 16b), however the intensity of R-π does not change when we vary the correlation length while holding the variance constant.

2.4.5 NEW Systems with the "right" amount of noise

For a better understanding of the reasons why R-π appears as it does in our simulated systems, we added a similar amount of noise to the model system as that seen in our simulations. Table 5 shows the amount of thermal noise in each dimension of the simulated system. We obtained those values by calculating the standard deviation in each dimension of the center of mass head group location from reference locations. We took the reference locations as the average center of mass of each head group. The standard deviations reported are only for frames over which we calculated the simulated diffraction patterns.

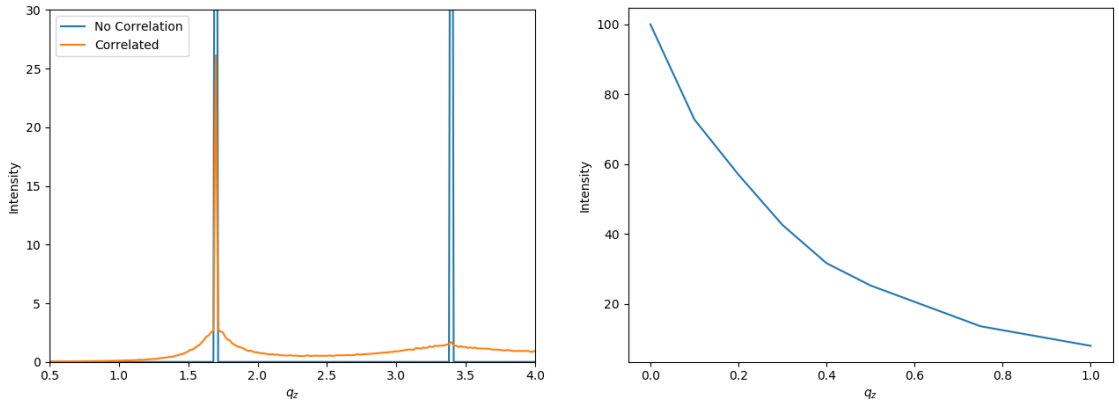

(a) (b)

Figure 15: (a) R-π broadens in the q_z direction when scatterers are correlated. (b) The intensity of R-π as the variance in scatterer position increases.

System	σ_x ($\mathring{A}$)	σ_y ($\mathring{A}$)	σ_z ($\mathring{A}$)
Sandwiched, Ordered	0.31	0.33	0.34
Parallel Displaced, Ordered	0.51	0.52	0.30
Sandwiched, Disordered	0.41	0.57	0.32
Parallel Displaced, Disordered	0.39	0.31	0.33

Table 5: Thermal noise in each dimension of the center of mass of monomer head groups for simulated LLC systems

Although the head groups do not move much in the equilibrated portion of the simulation, they are not arranged perfectly into columns. There is quenched disorder present from early in the simulation. To account for this noise, we measured the deviation of the center of masses from idealized positions. To calculate deviations in the x and y dimensions, we calculated the distance between each center of mass and the pore center. The distribution of the radial distance between each center of mass and the pore center, for the ordered sandwiched configuration, is shown in Figure 12a. To calculate deviations in the z dimension, we estimated the distance between layers to be the average z-box dimension divided by the number of scatterers per column (20 in the simulated system). Then we measured the deviation between the z position of each center of mass and its corresponding average z-layer position. Histograms of the deviations, for the ordered sandwiched configuration, are in Figure 12b. We use the standard deviation of each distribution in Figure 12 in order to place points in our model systems. The standard deviations for all systems are given in Table 6.

System	σ_r ($\mathring{A}$)	σ_z ($\mathring{A}$)
Sandwiched, Ordered	2.30	1.48
Parallel Displaced, Ordered	2.28	1.45
Sandwiched, Disordered	2.93	1.58
Parallel Displaced, Disordered	2.63	1.65

Table 6: Thermal noise in each dimension of the center of mass of monomer head groups for simulated LLC systems

For a good structural comparison, we set up a model system that mimics the ordered sandwiched configuration. We stacked scatterers 4.4 Åapart and created pores with a radius of 6.6 Åin order to be consistent with the values used to calculate the deviations in Table 6. We created an initial configuration with noise in

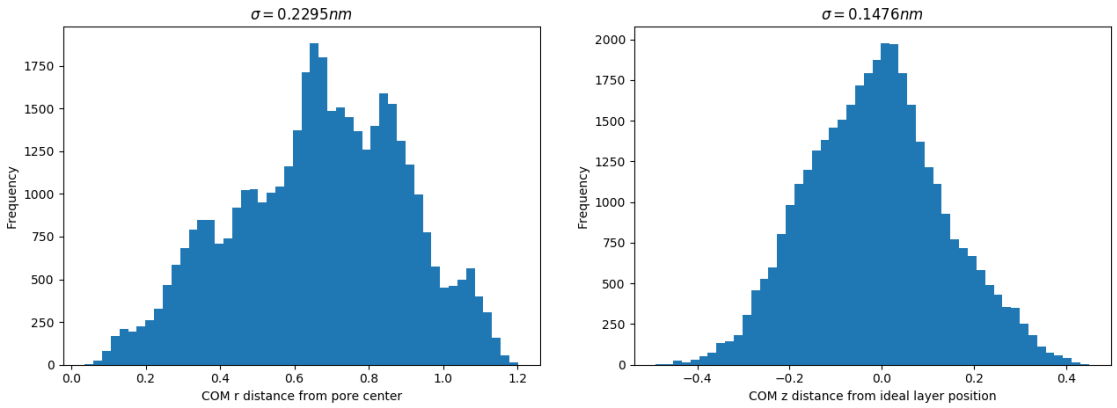

(a) (b)

Figure 16

the placement of points based on the values in Table 6. We made the scatterers correlated in the z-direction with a correlation length equal to 20 Åwhich is about what we've measured in the simulations. Using the initial configuration, we created 1000 frames to which we added thermal noise in accordance with that measured and recorded in Table 5. The result is a center-of-mass trajectory that is configured and behaves similarly to the simulation trajectory. We can use that model to tune the various influences on R-π.

The intensity of R-π is strongly dependent on the initial configuration. Each time a model system is generated, the initial configuration is different than the previous model system. The thermal noise added does not compensate for these differences. We ran 40 different model systems with the only difference being the initial randomization. The average R-π intensity of the 40 trials was 25.7 $\pm$ 9.4. This spread has important implications for the reproducibility of our data since there is velocity randomization during the initial equilibration. Also, this initial configuration dependence is not very useful for analyzing trends.

We observe the same R-π intensity when each frame of the trajectory is randomized. We created a trajectory of 1000 frames. We set up each frame as described in the paragraph before last, however with each frame independent. The average R-π intensity over 1000 frames was 25.4, in close agreement with that calculated for the 40 trials of 100 dependent configurations in the previous paragraph. We can use this type of setup to analyze trends.

Allowing columns to displace further with respect to each other causes the intensity of R-π to decrease (Figure **??**). In all of the above systems, we placed columns at exactly the same z displacement. Here we allowed them to displace from their initial centers as a function of the fraction of the distance between layers.

Qualitatively, we can make R-π look the most like experiment when columns move independently (See Figure **??**). As we decrease the dependence between columns, the intensity of R-π decreases and the reflection spreads out in the q_r direction. With any amount of dependence between columns, R-π sharpens at the center of the reflection.

Again, R-π decreases in response to thermal noise (See Figure **??**). We varied the amount of thermal noise from a 100 % decrease to a 100 % increase in noise in each dimension.

An increased correlation length causes a modest, linear increase in the intensity of R-π (Figure **??**). The effect is not nearly as pronounced as z-directional noise and column displacement.

As we increase the amount of noise in the initial, quenched disordered configuration, the intensity of R-π decreases (Figure **??**). We changed the amount of order in the initial configuration by scaling the noise used during placement from -100 % to 100 %. We scaled noise in all three dimensions, however we know that the maximum intensity of R-π will only be influenced by noise in the z direction.

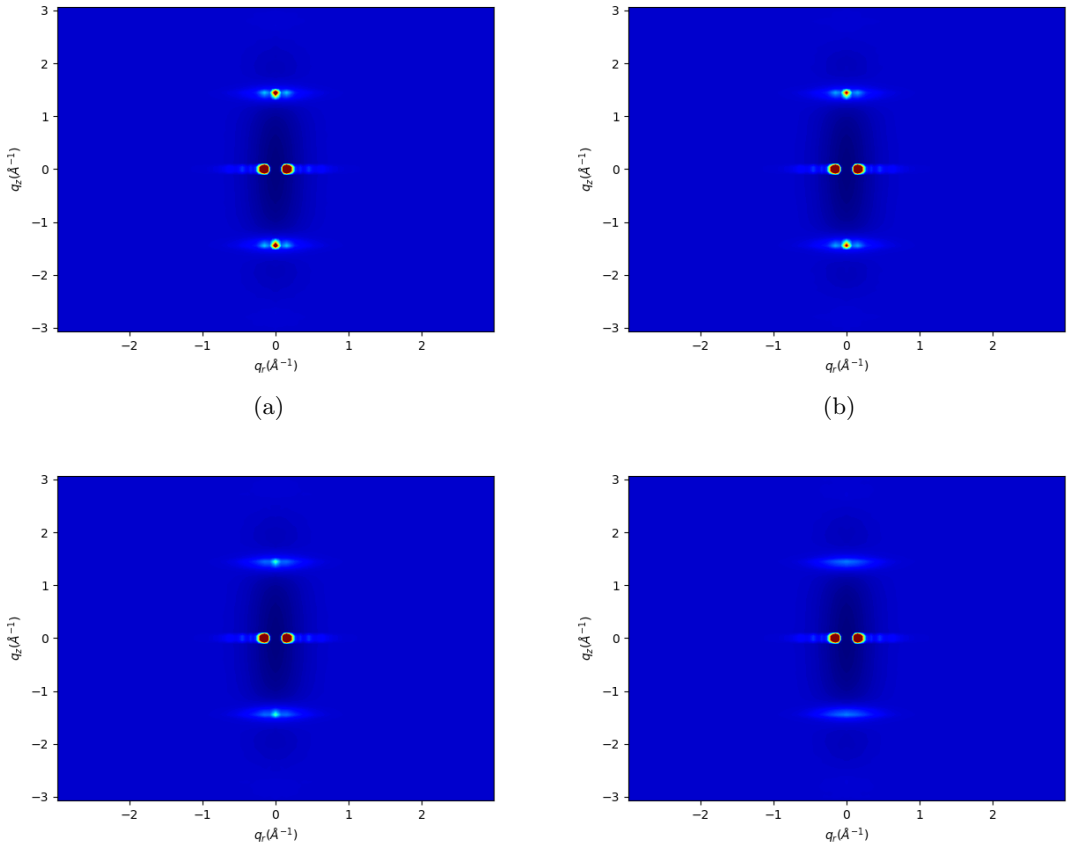

Figure 17: As we allow layers to move more independently, the intensity of R-π decreases and spreads out in the q_r direction.

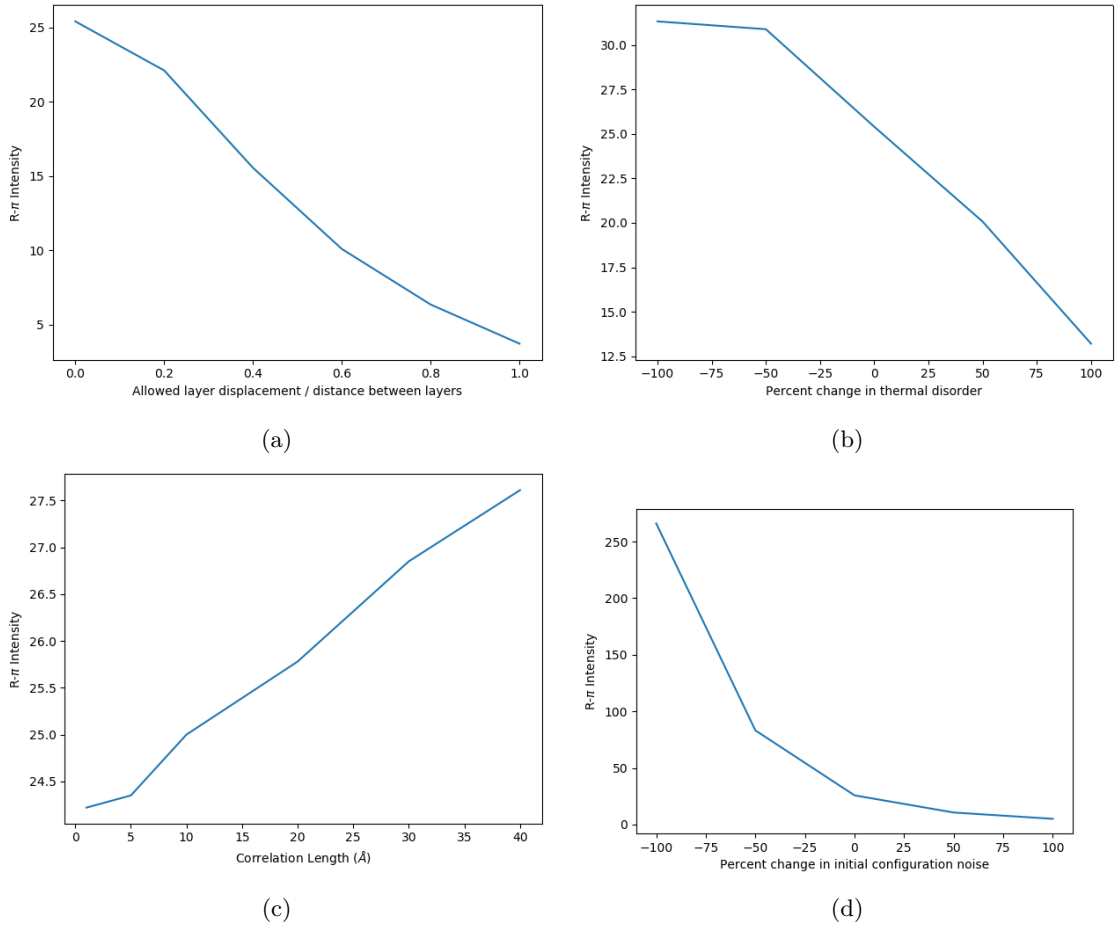

Figure 18: (a) The intensity of R-π decreases as the layers become more independent. (b) The intensity of R-π decreases when thermal disorder decreases. (c) The intensity of R-π increases with the correlation length. (d) The intensity of R-π decreases as more noise is added to the initial configuration.

3 Conclusion

A number of factors influence the shape and intensity of the R-π reflection. The maximum intensity of the reflection is most strongly influence by thermal disorder in the z-direction. The peak is broadened in the q_y (q_r) direction when there is xy-direction thermal disorder in systems with randomly displaced columns. The peak is broadened in the q_z direction when there is a finite (non-zero) correlation length between scatterers.